



# A New Close-Form Solution for Elastoplastic Seepage-Induced Stresses to Circular Tunnel with Considering Intermediate Principal Stress

Yu Zhao<sup>1</sup> · Tao Wei<sup>1</sup> · Chaolin Wang<sup>1</sup> · Jing Bi<sup>1</sup>

Received: 22 February 2023 / Accepted: 18 May 2023 / Published online: 14 June 2023  
© The Author(s), under exclusive licence to Springer-Verlag GmbH Austria, part of Springer Nature 2023

## Abstract

Based on the DP (Drucker–Prager) yield criterion, a new semi-analytical method for hydraulic–mechanical coupling in circular tunnels is proposed which takes into account the evolution of the permeability coefficient by incorporating it into the seepage equation. The definite condition is supplemented through the method of equal flow at the elastic–plastic junction. Constitutive equation and yield criterion are expressed by effective stress. When the pore water pressure drops to zero, the solution presented in this paper can degenerate into the classical Lamé solution in elastic region, and the solution obtained after yielding is consistent with the Drucker–Prager’s solution. The numerical simulation method is used to verify the proposed solution, and then, the sensitivity of the strength parameters is discussed. The results show that the radius of the plastic zone decreases with increasing cohesion  $C$  and internal friction angle  $\varphi^\circ$ , and the decreasing tendency is more sensitive at lower cohesion and internal friction angle. Higher initial yield stresses are easily obtained by increasing the values of these two parameters appropriately. The solution presented in this paper is not applicable when the internal friction angle is greater than  $40^\circ$ . Considering the intermediate principal stress, the solution presented in this paper shows a higher initial yield in-situ stress than that of MC (Mohr–Coulomb) and Hoek–Brown (HB) materials. Compared with the solution of DP criterion, the solution in the current work has a larger range of plastic region, and is more obvious in high in-situ stress area. In addition, the initial yield stress also increases linearly with the head loss.

## Highlights

- A new closed semi-analytical solution of hydraulic–mechanical coupling in circular tunnel is proposed using equivalent permeability coefficient.
- The hydraulic–mechanical coupling equation takes into account the action of intermediate principal stresses.
- The solution proposed in this paper can degenerate into the classical Lamé solution when pore water pressure is equal to zero.

**Keywords** Tunnel · Hydraulic–mechanical behavior · Permeability · Close-form solution

## List of Symbols

$\sigma$	Stress	$r$	Radius
$\varepsilon$	Strain	$Q$	Biot physical constant
$\varepsilon_v$	Volumetric strain	$\rho$	Density of water
$\lambda$	Lamé constant	$k$	Permeability coefficient
$G$	Shear modulus	$K_0$	Initial permeability
$u$	Displacement	$a$	Empirical constant
		$A_1, A_2$	Parameters of seepage equation
		$C_i$	Integration constant, $i = 1, 2, 3, 4$
		$I_1$	Stress first invariant
		$J_2$	The stress deviant is the second invariant
		$\beta, K$	The first and second strength parameters of DP rock mass

✉ Chaolin Wang  
chaolinwang@126.com

<sup>1</sup> College of Civil Engineering, Guizhou University, Huaxi District, Guiyang 550025, Guizhou, China

$\alpha$	Biot coefficient
$P$	Pore water pressure
$C$	Cohesion
$\varphi$	Internal friction angle
$n$	Pore volume
$n_0$	Initial pore volume
$\vartheta$	Pore outflow water

### Subscripts

$0, y, R$	Effective stress variable value at $r$ =tunnel periphery, elastoplastic interface, and outer boundary
$(e), (p)$	Elastic region function/variable, plastic zone function/variable
$r, \theta, z$	Direction of radial, tangential, and axial

## 1 Introduction

When the underground engineering below the groundwater table, the engineering is not only affected by the in-site stress, but also affected by the seepage force (De Caro et al. 2020; Li et al. 2022a; Wang et al. 2022a). Vice versa, engineering disturbance will cause mechanical response of surrounding rock and change the initial seepage field. In the above hydraulic–mechanical coupling process, the deformation and failure of the surrounding rock depend on the effective stress (Fransson and Viola 2021; Zhao et al. 2021; Wang et al. 2022b). The study of the hydraulic–mechanical coupling of underground tunnel is of guiding significance for the stability evaluation, support design, and cut-off/drainage design of the tunnel.

The analytical solutions of seepage and mechanics in the surrounding rock of circular tunnel have been studied extensively. Kolymbas and Wagner (2007) deduced the analytical solution of groundwater stable entry into tunnel by means of conformal mapping. Detournay and Cheng (1988) analyzed various coupled pore-elastic processes caused by vertical drilling in saturated formations under non-hydrostatic geostresses. Plastic failure of tunnel caused by high ground stress has attracted the attention of abundant scholars. Shin et al. (2011) studied the elastoplastic mechanical behavior of the tunnel caused by seepage with the MC failure criterion. Taking the seepage force as the volume force to evaluate the influence of pore water pressure on the stability of surrounding rock has been carried out in MC criterion (Bobet 2010; Lee et al. 2007; Shin et al. 2010) and HB materials (Fahimifar and Zareifard 2009; Sharan 2005; Zareifard and Fahimifar 2014). According to the plane strength theory, the intermediate principal stress is ignored in the above studies, and the calculation results of stress tend to be conservative.

Deep-buried circular tunnel is usually accompanied by high ground stress, which will cause the yield failure

at the periphery of the tunnel. To simplify the process of fluid–structure coupling modeling, stress superposition or the seepage equation of fixed state is considered. To simplify the process of groundwater hydraulic–mechanical coupling modeling, stress superposition method (Wang and Dusseault 1994) or the specific seepage equation (Zhang et al. 2019) is considered. Zareifard and Fahimifar (2014) deduced the elastoplastic solution of a circular tunnel under steady flow by assuming a constant permeability coefficient. Related to the change of effective stress, the deformation and failure of surrounding rock change the permeability which is consistent with the experimental results of previous study (Chen et al. 2007; Wang et al. 2013; Xu and Yang 2016; Yang et al. 2015; Zhao et al. 2022; Zhang et al. 2023). Fahimifar and Zareifard (2013) deduced the distribution of strain-dependent permeability. According to the method of permeability proportion fraction, Dong et al. (2019) generalized the evolution law of permeability coefficient in elastic zone and plastic zone, so as to establish the hydraulic–mechanical coupling model. When the permeability coefficient changes along the seepage path, the flow velocity often depends on the part with the lowest permeability. However, in the previous studies, this detail is often ignored, which may lead to a larger calculation result.

In this paper, the permeability coefficient is a non-constant parameter in the calculation of coupling. According to the deformation characteristics, the permeability coefficient evolution model and the seepage model in the elastic and plastic zone are established, respectively. Based on the conservation of fluid mass and the physical relation between the equivalent permeability coefficient and the head loss, a new closed solution for circular tunnel with fluid–structure coupling was proposed. Considering the effect of intermediate principal stress, the hydraulic–mechanical coupling model with DP criterion is derived. Finally, the derived stress solution is verified by numerical simulation method.

## 2 Background Study and General Theory

### 2.1 General Theory and Assumptions

In this study, the mechanical problem of a circular underground tunnel is identified as a two-dimensional plane strain model. Surrounding rock in the range of inner diameter  $r_0$  to outer diameter  $r_R$  is assumed to be homogeneous isotropic and the plastic volume is considered incompressible. The assumption of incompressibility of the plastic volume is used to simplify the effect of plastic strain on the change in pore volume and thus obtain a solvable differential equation. Such an assumption would neglect the contribution of plastic strain to pore alteration after yielding of the surrounding rock. Changes in porosity are thought to be exponential to permeability. The

intermediate principal stress can be represented by two other stress components in the plane, so that the stress differential equation satisfying the DP failure criterion has an analytical solution. The outer boundary is subjected to uniform in-situ stress  $\sigma_R$  and pore water pressure  $P_R$ . Axial stress is considered to be the intermediate value between radial stress and tangential stress. The effective stress is applied in DP yield criterion to determine the plastic zone range and stress distribution of surrounding rock. The DP yield criterion expressed by effective stress can be expressed as follows:

$$F(I'_1, \sqrt{J'_2}) = \sqrt{J'_2} - \beta I'_1 - K = 0, \tag{1}$$

where  $I'_1$  and  $J'_2$  are the first invariants of stress tensor and the second invariants of deviatoric tensor of stress expressed by effective stress, respectively, which are defined as follows:

$$I'_1 = \sigma'_r + \sigma'_\theta + \sigma'_z \tag{2}$$

$$J'_2 = \frac{1}{6} [(\sigma'_r - \sigma'_\theta)^2 + (\sigma'_\theta - \sigma'_z)^2 + (\sigma'_z - \sigma'_r)^2]. \tag{3}$$

Effective stress is defined as follows:

$$\sigma'_\theta = \sigma_\theta - \alpha P \quad \sigma'_r = \sigma_r - \alpha P \quad \sigma'_z = \sigma_z - \alpha P, \tag{4}$$

where  $\alpha$  is the Biot coefficient, which generally depends on the volume modulus of surrounding rock and solid granular material (in this solution,  $\alpha$  is regarded as a constant);  $P$  is pore water pressure; the subscripts  $\theta$ ,  $r$ , and  $z$  refer to the tangential, radial, and axial directions, respectively. For example,  $\sigma_r$  represents radial stress. In DP yield criteria,  $\beta$  and  $K$  are strength parameters related to friction angle and cohesion, which are defined as follows (Kabwe et al. 2020):

$$K = \frac{6C \cos \varphi}{\sqrt{3}(3 - \sin \varphi)} \tag{5}$$

$$\beta = \frac{6 \sin \varphi}{\sqrt{3}(3 - \sin \varphi)}, \tag{6}$$

where  $\varphi$  is the internal friction angle and  $C$  is the cohesion force. In the case of the assumption of plasticity incompressible, the plastic incompressible plane strain model has the following relation:

$$\sigma_z = \frac{\sigma_r + \sigma_\theta}{2}. \tag{7}$$

### 2.2 Governing Equations

The schematic diagram of stress of a deeply buried tunnel in a saturated formation is shown in Fig. 1. In the figure, subscript

$r$  is the distance to the center of the circle, and the subscripts 0,  $y$ , and  $R$  represent the periphery, the elastoplastic interface, and the outer boundary, respectively. The rock skeleton is considered to be elastically compressible and is specified to be positive for compression and negative for tension. Assuming that the pore water pressure only bears positive stresses and has no effect on shear stresses, the constitutive equations can be expressed by the following equation:

$$\begin{cases} \sigma_r = \lambda \varepsilon_v + 2G\varepsilon_r + \alpha P \\ \sigma_\theta = \lambda \varepsilon_v + 2G\varepsilon_\theta + \alpha P \end{cases}, \tag{8}$$

where  $\lambda$  and  $G$  are the Lamé constants, and  $\varepsilon_r$ ,  $\varepsilon_\theta$ , and  $\varepsilon_v$  are the radial, tangential, and volume strain, respectively. The volumetric strain and geometric equations and the equilibrium equation in the plane strain axisymmetric problem have the following form:

$$\varepsilon_r = \frac{\partial u}{\partial r}, \quad \varepsilon_\theta = \frac{u}{r} \tag{9}$$

$$\varepsilon_v = \varepsilon_r + \varepsilon_\theta = \frac{\partial u}{\partial r} + \frac{u}{r} = \frac{1}{r} \frac{\partial(ru)}{\partial r} \tag{10}$$

$$\frac{\partial \sigma_r}{\partial r} + \frac{\sigma_r - \sigma_\theta}{r} = 0, \tag{11}$$

where  $u$  is radial displacement.

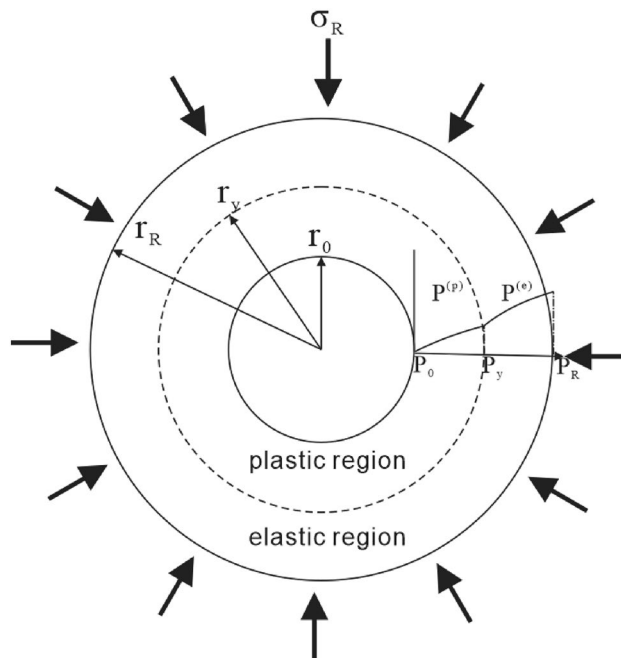


Fig. 1 Hydraulic–mechanical calculation model of a circular tunnel

### 2.3 Basic Problems of Hydraulic–Mechanical Coupling

The key point of hydraulic–mechanical coupling is to establish the dynamic mathematical model of pore volume  $n$  and permeability coefficient  $k$ . To solve seepage problems in circular cavity, previous studies mainly treat the seepage force of a fixed potential as a volume force (Fahimifar and Zareifard 2013; Li et al. 2022b). This obviously ignores the effect of rock compression on permeability. Assuming that water is incompressible, the change in volume of the rock  $\Delta V$  equals the change in pore volume  $\Delta n$ , and also equals the water content of the outflow  $\vartheta$ . The change in water content has the following expression (Biot 1941):

$$\Delta V = \Delta n = \vartheta = \frac{P}{Q} - \alpha \varepsilon_v. \quad (12)$$

In an isotropic homogeneous porous elastic medium, the permeability is a function of the pore volume. Xu et al. (2000) presented an exponential relationship between the permeability coefficients  $k$  and pore volume  $n$

$$k(n) = k_0 e^{an} = K_0 e^{a\Delta n}, \quad K_0 = k_0 e^{an_0}, \quad (13)$$

where  $a$  is an empirical constant and  $k_0$  is the initial intrinsic permeability. Substituting Eq. (12) into Eq. (13) yields the following equation, which is the basis for solving the nonlinear seepage and flow coupling problem later:

$$k(n) = K_0 e^{a\left(\frac{P}{Q} - \alpha \varepsilon_v\right)}. \quad (14)$$

The nonlinear Darcy seepage equation and the continuity equation have the following forms:

$$q = k(n) \frac{\partial P}{\partial r} \quad (15)$$

$$\nabla \left( \rho k(n) \frac{\partial P}{\partial r} \right) = n_0 \frac{\partial P}{\partial t} + \frac{1}{Q} \frac{\partial(\rho P)}{\partial t} - \alpha \frac{\partial(\rho \varepsilon_v)}{\partial t}, \quad (16)$$

where  $\rho$  denotes water density which is assumed as incompressible (i.e.,  $\rho$  is a constant). The continuous equation of stable seepage for two-dimensional axisymmetric incompressible fluid can be simplified as follows:

$$\frac{1}{r} \frac{d}{dr} \left[ rk(n) \frac{dP}{dr} \right] = 0. \quad (17)$$

Substituting the constitutive Eq. (8) into the equilibrium Eq. (11), obtains the equilibrium equation with pore pressure. To solve the equilibrium equation, the basic differential equation for solving stress can be obtained using Eq. (10)

$$\frac{d}{dr} \left\{ \frac{1}{r} \frac{d(ru)}{dr} \right\} = - \frac{\alpha}{\lambda + 2G} \frac{dP}{dr}. \quad (18)$$

Equations (17) and (18) are the basic differential equations of seepage and mechanics. Obviously, they are coupled and cannot be solved separately. After obtaining the displacement  $u$  and pore water pressure  $P$ , the stress and strain can be solved by solving the geometric equation and constitutive equation. When the stress exceeds the yield strength of the surrounding rock, a plastic yield zone is generated first at the periphery of the tunnel. For the case of plastic damage, the fixed solution conditions are more demanding and the boundary conditions on the elastic–plasticity need to be considered. The percolation conditions and mechanical behavior of the plastic zone are altered, and these are discussed in the next section.

### 2.4 Boundary Conditions

The tangential and radial stresses at the outer boundary are equal to the in-situ stress  $\sigma_R$ . At the inner boundary, the support force is  $\sigma_0 = 0$ . A constant head boundary is set at outer boundaries, water flowing inwards from the outer boundary. The radial stress and pore water pressure are continuous at the junction of the elastoplastic region. Thus, the boundary conditions can be expressed as follows:

$$\begin{cases} \sigma_r = \sigma_\theta = \sigma_R, P = P_R & (r = r_R) \\ \sigma_r = \sigma_r^{(e)} = \sigma_r^{(p)} = \sigma_y, P = P_y & (r = r_y) \\ \sigma_r = \sigma_0 = 0, P = P_0 = 0 & (r = r_0) \end{cases}. \quad (19)$$

### 2.5 Hydraulic Problem

Carrying out one integral calculation of Eq. (18) and combining with the definition of the pore volume increment in Eq. (12) yield

$$\Delta n = \left( \frac{1}{Q} + \frac{\alpha}{\lambda + 2G} \right) P + \alpha C_1, \quad (20)$$

where  $C_1$  is the integration constant, which can be obtained using the boundary conditions at  $r_R$

$$C_1 = \frac{\sigma_R - \alpha P_R}{\lambda + G} + \frac{\alpha}{\lambda + 2G} P_R. \quad (21)$$

The total volume strain of the plastic zone is  $\varepsilon_v = \varepsilon_v^{(e)} + \varepsilon_v^{(p)}$ . Due to the assumption of plasticity incompressible, the plastic strain has no effect on the change of pore volume. For a completely plastic material,  $\varepsilon_v^{(e)} = \text{const}$  after yielding. Substituting Eqs. (20) and (21) into Eq. (13) yields

$$k^{(e)}(n) = K_0 e^{\left[ a \left( \frac{1}{Q} + \frac{\alpha}{\lambda + 2G} \right) P + \alpha \left( \frac{\sigma_R - \alpha P_R}{\lambda + G} + \frac{\alpha}{\lambda + 2G} P_R \right) \right]} \tag{22}$$

Equation (22) is substituted into Eq. (17) to obtain the seepage differential equation in the elastic zone

$$\frac{1}{r} \frac{d}{dr} \left[ r e^{A_1 P^{(e)}} \frac{dP^{(e)}}{dr} \right] = 0. \tag{23}$$

Similar to the plastic zone, the equations for permeability coefficient and the differential equations seepage can be obtained as

$$k^{(p)}(r) = K_0 e^{a \left[ \frac{P}{Q} + \alpha \varepsilon_v^{(e)} \right]} \tag{24}$$

$$\frac{1}{r} \frac{d}{dr} \left[ r e^{A_2 P^{(p)}} \frac{dP^{(p)}}{dr} \right] = 0, \tag{25}$$

where  $A_1 = a \left( \frac{1}{Q} + \frac{\alpha}{\lambda + 2G} \right)$ ,  $A_2 = \frac{\alpha}{Q}$ . From the above derivation process, for the elastic and plastic seepage equations under steady-flow conditions, the difference lies mainly in the different permeability coefficients. The pore volume change in the elastic zone is affected by volume strain and pore water pressure, while that in the plastic zone is only affected by pore water pressure. The permeability coefficient  $k$  is continuous in the elastic zone and the plastic zone with an inflection point at  $r$  elastic–plastic junction. In general, the closer to the periphery of the tunnel, the more rock strain before plastic yielding, resulting in a lower permeability coefficient.

### 3 Solution of Nonlinear Flow Coupling Problem Based on DP Criterion

#### 3.1 Stress Solution

The stresses in the elastic zone are solved by integrating Eq. (18) twice

$$u^{(e)}(r) = -\frac{\alpha}{\lambda + 2G} \frac{1}{r} \int_{r_y}^r P^{(e)}(r') r' dr' + \frac{C_2}{2} \left( r + \frac{r_y^2}{r} \right) + \frac{r_y}{r} C_3, \tag{26}$$

where  $C_2$  and  $C_3$  are the integration constants, and  $r_y$  indicates the radius of the plastic area,  $r$  is a integration variable. Bringing the boundary conditions at the outer boundary  $r_R$  and the elastoplastic junction  $r_y$  into the geometric equations and the intrinsic equations, yields

$$C_2 = \frac{1}{(\lambda + G)} \left[ \frac{\sigma_R R^2 - \sigma_y r_y^2}{R^2 - r_y^2} - \frac{2\alpha G}{\lambda + 2G} \frac{1}{R^2 - r_y^2} \int_{r_y}^R P^{(e)}(r') r' dr' \right], \tag{27}$$

where

$$C_3 = C_2 \left[ 1 + \frac{\lambda}{2G} \right] r_y - \frac{\sigma_y r_y}{2G} \tag{28}$$

$$\sigma_r^{(e)}(r) = \frac{2\alpha G}{\lambda + 2G} \left[ \frac{1}{r^2} \int_{r_y}^r P^{(e)}(r') r' dr' - \frac{1}{R^2 - r_y^2} \left( 1 - \frac{r_y^2}{r^2} \right) \int_{r_y}^R P^{(e)}(r') r' dr' + \frac{\sigma_R R^2 - \sigma_y r_y^2}{R^2 - r_y^2} - \frac{(\sigma_R - \sigma_y) R^2 r_y^2}{(R^2 - r_y^2) r^2} \right] \tag{29}$$

$$\sigma_\theta^{(e)}(r) = \frac{2\alpha G}{\lambda + 2G} \left[ P - \frac{1}{r^2} \int_{r_y}^r P^{(e)}(r') r' dr' - \frac{1}{R^2 - r_y^2} \left( 1 + \frac{r_y^2}{r^2} \right) \int_{r_y}^R P^{(e)}(r') r' dr' + \frac{\sigma_R R^2 - \sigma_y r_y^2}{R^2 - r_y^2} + \frac{(\sigma_R - \sigma_y) R^2 r_y^2}{(R^2 - r_y^2) r^2} \right] \tag{30}$$

Equations (29) and (30) are the elastic solutions of the radial and tangential stresses. It is worth mentioning that the first term on the right-hand side of both equations is related to the pore water pressure, and the elastic solutions degenerate to the classical Lamé solution when the pore water pressure  $P$  is kept constant equal to 0.

Plastic deformation occurs when the stress in the surrounding rock meets the yield condition of Eq. (1). The simple transformation of yield conditions is made by combining Eqs. (1)–(7)

$$\sigma_r - \sigma_\theta = -\frac{6\beta}{1 + 3\beta} \left( \sigma_r - \alpha P^{(p)} + \frac{K}{3\beta} \right). \tag{31}$$

Substituting Eq. (31) into the equilibrium Eq. (11) yields the differential equation for solving the plastic stress

$$\frac{d\sigma_r}{dr} - \frac{6\beta}{1 + 3\beta} \left( \sigma_r - \alpha P^{(p)} + \frac{K}{3\beta} \right) \frac{1}{r} = 0. \tag{32}$$

Integrating the above equation once and making  $M = \frac{6\beta}{1 + 3\beta}$  yields

$$\sigma_r^{(p)}(r) = \left[ \int \left( -\frac{M}{3\beta} (3\alpha P^{(p)} \beta - K) r^{-M-1} \right) dr + C_4 \right] r^M. \tag{33}$$

The constant of integration  $C_4$  can be eliminated using the inner boundary condition

$$C_4 = \frac{\sigma_0}{r_0^M}. \tag{34}$$

Then, Eq. (33) can be expressed as

$$\sigma_r^{(p)}(r) = \left[ -\alpha M \int_{r_0}^r P_r^{(p)} r^{(-M-1)} dr - \frac{K}{3\beta} (r^{-M} - r_0^{-M}) + \frac{\sigma_0}{r_0^M} \right] \cdot r^M. \tag{35}$$

Considering the yield condition Eq. (31), one can obtain the tangential stress in the plastic zone

$$\sigma_\theta^{(p)}(r) = \sigma_y(1 + M) + M \left( \frac{K}{3\beta} - \alpha P_y \right). \tag{36}$$

### 3.2 Hydraulic Solution

The basic differential equations for seepage in the elastic and plastic zones have been discussed above, and this section further solves these differential equations. The solution of the equation for seepage in the elastic zone requires integrating Eq. (23) twice and then eliminating the integration constants using the first and second terms of Eq. (19) (boundary conditions outside the elastic zone and boundary conditions inside the elastic zone). Similarly, Eq. (25) is integrated twice, and then, the integration constants are eliminated using the second and third terms of Eq. (19) (boundary conditions outside the plastic zone and boundary conditions inside the plastic zone).

The seepage equation in the elastic region can be obtained

$$P^{(e)}(r) = \frac{1}{A_1} \ln \left( \frac{e^{A_1 P_R} - e^{A_1 P_y}}{\ln \frac{R}{r_y}} \ln \frac{r}{r_y} + e^{A_1 P_y} \right). \tag{37}$$

Similarly, the seepage equation in the plastic zone is

$$P^{(p)}(r) = \frac{1}{A_2} \ln \left( \frac{e^{A_2 P_y} - e^{A_2 P_0}}{\ln \frac{r_y}{r_0}} \ln \frac{r}{r_0} + e^{A_2 P_y} \right). \tag{38}$$

Because the second term of Eq. (19) is applied in the solution of both Eqs. (37) and (38), it is obvious to obtain the conclusion that the pore water pressure is equal at the junction of the elastic and plastic zones. Since the pore water pressure  $P$  is indicated here to be identical, additional conditions need to be found to seal the coupled system.

### 3.3 Coupled Equations

After solving seepage equation in the elastoplastic region, the pore water pressure  $P$  in the stress Eqs. (29), (30), (35),

and (36) has a specific expression. In solving the stress equation for the plastic zone, only the inner boundary conditions are used, so here the following relationship can be obtained using the condition that the radial and tangential stresses at  $r_y$  are equal:

$$\sigma_y = \left[ -\alpha M \int_{r_0}^{r_y} P^{(p)}(r) r^{(-M-1)} dr - \frac{K}{3\beta} (r_y^{-M} - r_0^{-M}) + \frac{\sigma_0}{r_0^M} \right] \cdot r_y^M \tag{39}$$

$$\sigma_\theta^{(e)}(r_y) = \sigma_y(1 + M) + M \left( \frac{K}{3\beta} - \alpha P_y \right). \tag{40}$$

The two equations above have three unknown parameters  $r_y$ ,  $\sigma_y$ , and  $P_y$ . Obviously, the system of equations is not closed. However, the boundary condition at  $r_y$  for pore water  $P$  has already been used in the solution of the seepage equation.

Figure 2 shows the alternating aquifers in the seepage path, each with independent permeability coefficients. In this case, the water flow is equal in each aquifer, the hydraulic slope of each aquifer is different, and the total hydraulic slope is equal to the sum of the head loss of each aquifer

$$Q = k_i A \frac{\Delta P_i \rho g}{L_i}, \quad \Delta P_i = \frac{L_i Q}{k_i A \rho g}. \tag{41}$$

If an equivalent homogeneous aquifer is used to replace the “strung” aquifer, this homogeneous aquifer has an equivalent permeability coefficient of  $k_e$

$$k_e = \frac{\sum_{i=1}^n k_i L_i}{\sum_{i=1}^n L_i}. \tag{42}$$

If the aquifer is sufficiently thin and the permeability coefficients of adjacent aquifers are gradually transformed, the equivalent permeability coefficient can be expressed as

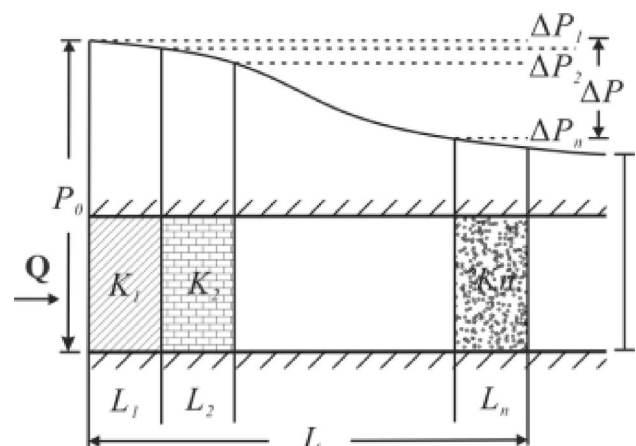


Fig. 2 “Strung” aquifer seepage model



$$k_e = \frac{1}{M} \int_0^L K(l)dl. \tag{43}$$

Figure 3 shows the relationship of permeability coefficient  $k$  with radius  $r$ . The surrounding rock is assumed to be a uniformly homogeneous porous elastic medium, and the pore volume changes with stress and pore water pressure. The seepage behavior no longer satisfies the linear Darcy’s law. In the previous analysis, it was concluded that  $k$  is continuous over the elastic and plastic regions, respectively, and equal at  $r_y$ . Similarly, the elastic zone equivalent permeability coefficient and the plastic zone equivalent permeability coefficient can be defined as follows:

$$k_e^{(e)} = \frac{1}{R - r_y} \int_{r_y}^R e^{A_1 P^{(e)}} dr, \quad k_e^{(p)} = \frac{1}{r_y - r_0} \int_{r_0}^{r_y} e^{A_2 P^{(p)}} dr. \tag{44}$$

According to the law of mass conservation, the flow rate at the elastic–plastic junction is equal, so that the following relationship can be obtained by:

$$\frac{k_e^{(e)}}{k_e^{(p)}} = \frac{\Delta P^{(e)}}{\Delta L^{(e)}} \cdot \frac{\Delta L^{(p)}}{\Delta P^{(p)}} = \frac{P_R - P_y}{R - r_y} \cdot \frac{r_y - r_0}{P_y - P_0}. \tag{45}$$

Equation (45) is now supplemented with the relational equation on  $P_y$  and  $r_y$ . The closed system of coupled equations can be formed by combining Eqs. (39) and (40). Since it contains transcendental equations, this system of equations cannot be solved directly and needs to be solved with the help of numerical methods. After solving  $r_y, P_y$ , and  $\sigma_y$ , the corresponding solutions are obtained by substituting the stress equation and the seepage equation.

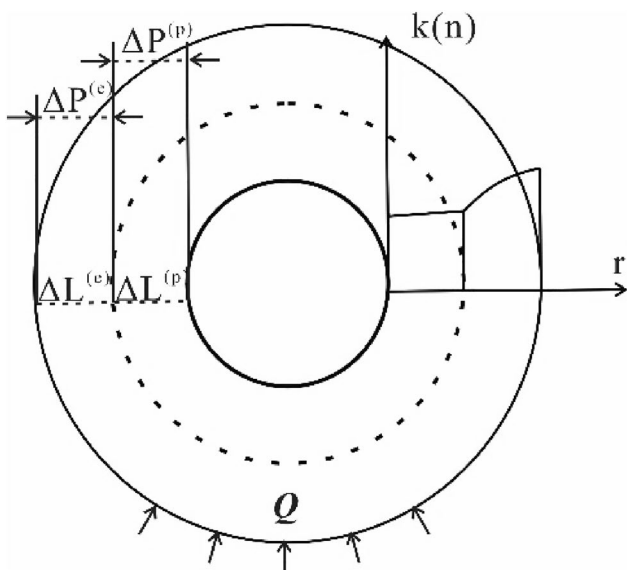


Fig. 3 Circular continuous aquifer seepage model

When the stress at  $r_0$  reaches the yield condition, we have

$$\sigma_\theta = \frac{2K}{1 - 3\alpha}. \tag{46}$$

Substituting Eq. (30) into Eq. (46), the in-situ stress at the beginning of yield can be obtained by:

$$\sigma_R = \left\{ \frac{K}{1 - 3\alpha} - \frac{2G}{\lambda + 2G} \left[ P_0 - \frac{2}{R^2 - r_0^2} \int_{r_0}^R P^{(e)}(r)rdr \right] \right\} \frac{R^2 - r_0^2}{R^2}. \tag{47}$$

## 4 Model Verification

### 4.1 Comparison with Numerical Simulation Test Results

In this part, FLAC3D were adopted to conduct numerical tests with the DP failure criterion. The convergence of the numerical results was discussed as follows. Since the numerical model is a planar axisymmetric model, the number of circumferential grids has little effect on the test results, so the sensitivity analysis can be carried out only using the radial grids. The model with different numbers of radial meshes  $N$  is calculated to investigate the effect of the discretization number. The number of steps at each computational convergence is recorded, and the unbalanced forces rate is used to mark the convergence. The iteration error  $e_n$  is estimated by calculating the average stress difference. The results of the grid sensitivity analysis are recorded in Table 1.

Figure 4 shows how the iteration error gradually converges as the number of grids increases, with the party

Table 1 Results of the grid sensitivity analysis

$N$	Step	Unbalance force rate	$e_n$
20	5623	9.99E-06	–
30	6592	1.00E-05	0.01738
40	8379	1.00E-05	0.00769
50	10,106	9.99E-06	0.00526
60	12,034	9.98E-06	0.00392
70	13,991	9.99E-06	0.00279
80	16,121	9.98E-06	0.00229
90	18,335	9.99E-06	0.00196
100	20,585	1.00E-05	0.00155
110	22,656	9.99E-06	0.00104
120	25,055	1.00E-05	9.94E-04
130	27,097	1.00E-05	8.66E-04
140	29,220	1.00E-05	8.38E-04
150	31,370	9.99E-06	8.25E-04

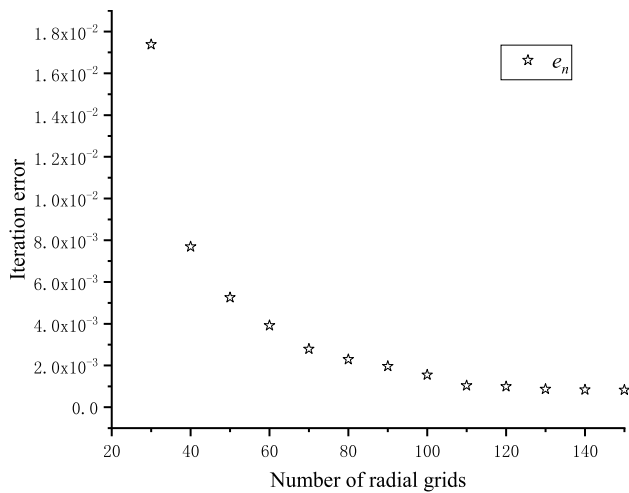


**Fig. 4** Iterative error distribution

$e_n = 2 \times 10^{-3}$  iteration error starting to converge. Taking into account of the computational accuracy and computational cost, the radial grid number of 80 was chosen for this experiment.

The numerical model generated  $80 \times 20 \times 4$  'cshell zone', and applied 30 and 60 MPa normal stress on the outer boundary, and initialized pore pressure and boundary condition by Eq. (19). The nodal displacements perpendicular to the plane direction were fixed to simulate a plane strain model. The inner boundary of the tunnel is 10 m and the outer boundary is 40 m. Calculated model with friction angle  $\varphi = 25^\circ$ , cohesion  $C = 6$  MPa, and shear modulus  $G = 2.5 \times 10^3$  MPa. DP criterion parameter  $qv = \frac{2 \sin(\phi)}{\sqrt{3(3-\sin(\phi))}}$ ,  $ks = \frac{6C \cos \phi}{\sqrt{3(3-\sin(\phi))}}$ . The numerical model, plastic-elastic distribution, and colored stress patterns are shown in Fig. 5.

Figure 6 shows the stress distribution of surrounding rock obtained from simulation tests and the calculated results under the conditions of 30 MPa and 60 MPa in-situ stress  $\sigma_R$ . As can be seen from the figure, the simulated and calculated radial stress results are basically the same, no matter in the elastic zone or the plastic zone, while the simulated tangential stress results in the plastic zone are slightly higher than that of calculated tangential stress. Under the condition of  $\sigma_R = 30$  MPa, the two obtained results are almost the same. Under the condition of  $\sigma_R = 60$  MPa, the plastic zone radius of simulated tests is slightly smaller than that of calculated results. In general, the theoretical calculation results of this paper are in good agreement with the numerical test results.

Based on the comparative analysis results of Sects. 4.1 and 4.2, we can preliminarily believe that the theoretical derivation in this paper is reasonable and correct.

## 4.2 Comparison with the Solution Without Considering the Seepage Effect

The stress distribution diagram of DP and this work is shown in Fig. 7. Both the low and the high in-situ stress show similar feature. In the plastic zone, the stress distribution under the two yield criteria is basically the same, but the solution in this paper shows a larger range of the plastic zone. In the elastic zone, the tangential stress curves of the two solutions are basically parallel. In addition, the radial stress given in this paper is also higher than the solution of DP, but different from tangential stress, the difference of radial stress is the smallest at  $r_y$ , gradually increases with the increase of radius, and reaches the maximum at  $r_R$ . This is positively correlated with the distribution of pore water pressure. These differences are magnified in areas of high in-situ stress.

Based on the comparative analysis results of Sects. 4.1 and 4.2, we can preliminarily believe that the theoretical derivation in this paper is reasonable and correct.

## 5 Example Analysis

In this part, we make some examples to study the influence of different parameters on the results, and give the following calculation parameters. The inner diameter of the tunnel  $r_0 = 10$  m;  $R = 4 \times r_0$ , the friction angle in the zone  $\varphi = 25^\circ$ , the cohesion  $C = 6$  MPa, the Biot coefficient  $\alpha = 0.3$ , the Lamé constant  $\lambda = 1.445$ , the shear modulus  $G = 2.5 \times 10^3$  MPa, and the empirical constant  $a = 1$ ,  $Q = 1536 \times 103$ .

(1) The relationship between the in-situ stress and the radius rate of the plastic zone under the same conditions for the four yielding criteria is shown in Fig. 8. Pore water pressure of 10 MPa is applied at the outer boundary. There are some differences in the performance of the initial yield stress and the growth rate of the plastic zone radius. As this work is carried out based on DP criterion, the calculation results are highly familiar to the DP algorithm. However, under the action of pore water pressure, in the solution of current work, the increase of plastic zone radius shows a higher sensitivity to the growth of in-situ stress. It can be seen from the figure that DP, HB, and the solution in this paper have similar slopes, while Kastner's solution is more sensitive to high ground stress. In addition, due to the intermediate principal stress considered by both DP and this work, the obtained results have higher initial yield stress than HB and Kastner's solutions. In the HB criterion parameters  $m = 10$  and  $s = 1$ ; the same parameters are used in the calculation procedure of the DP criterion for uncoupled seepage action as in this study. The solution in this study has an inner boundary water



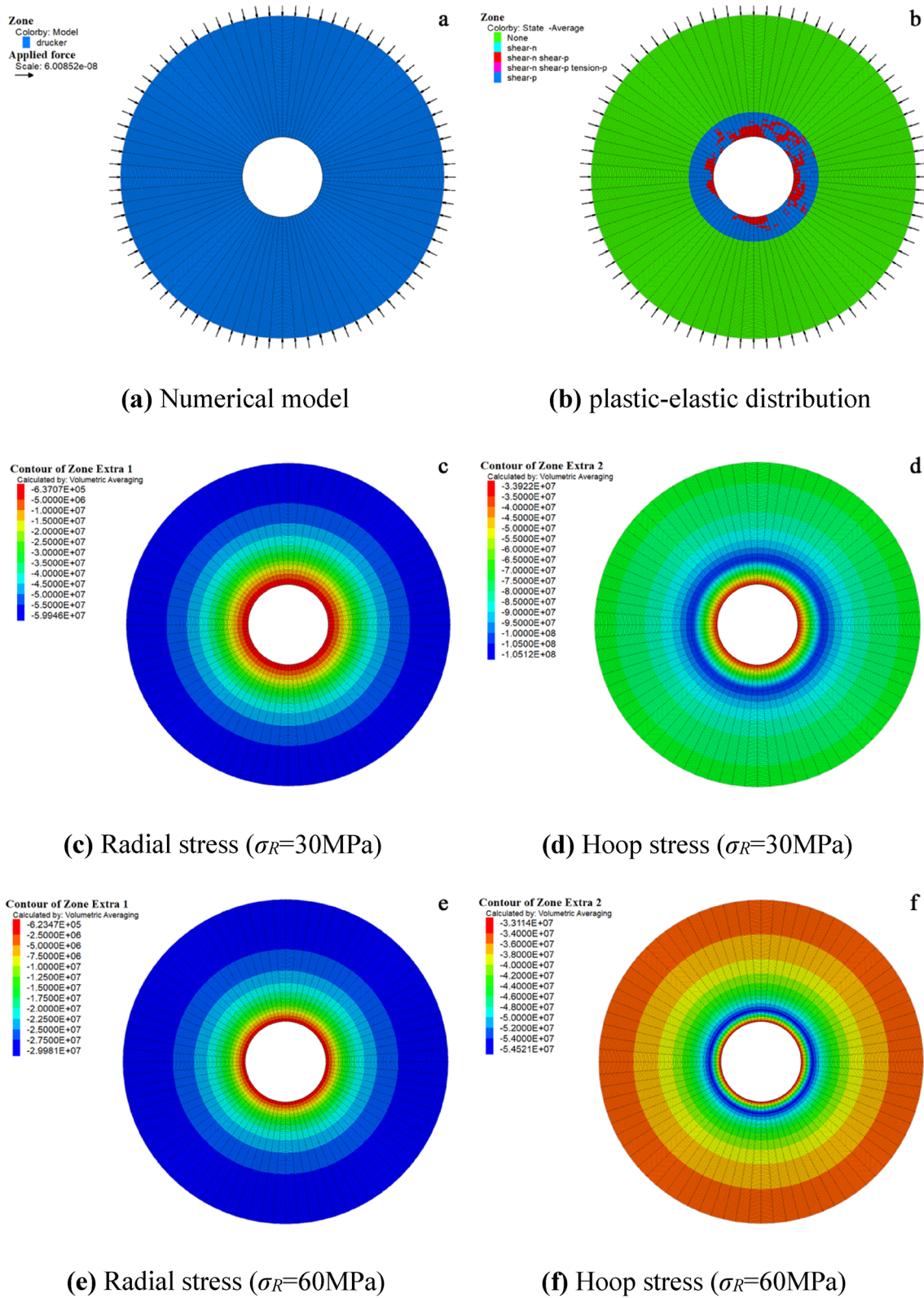
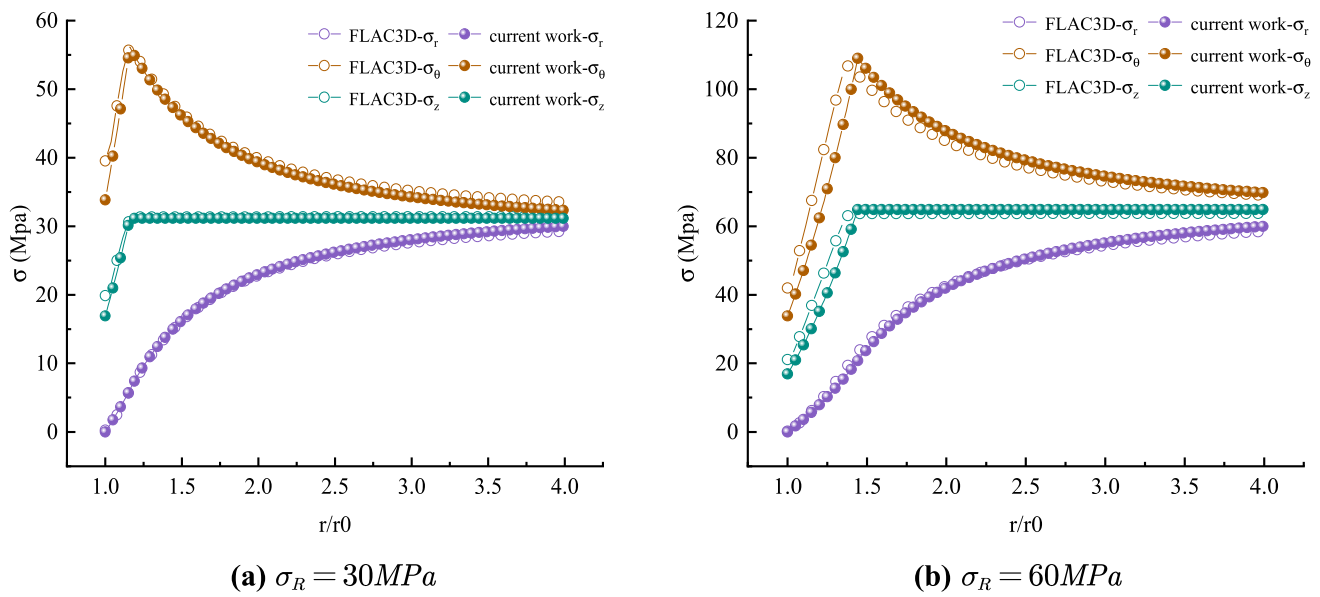
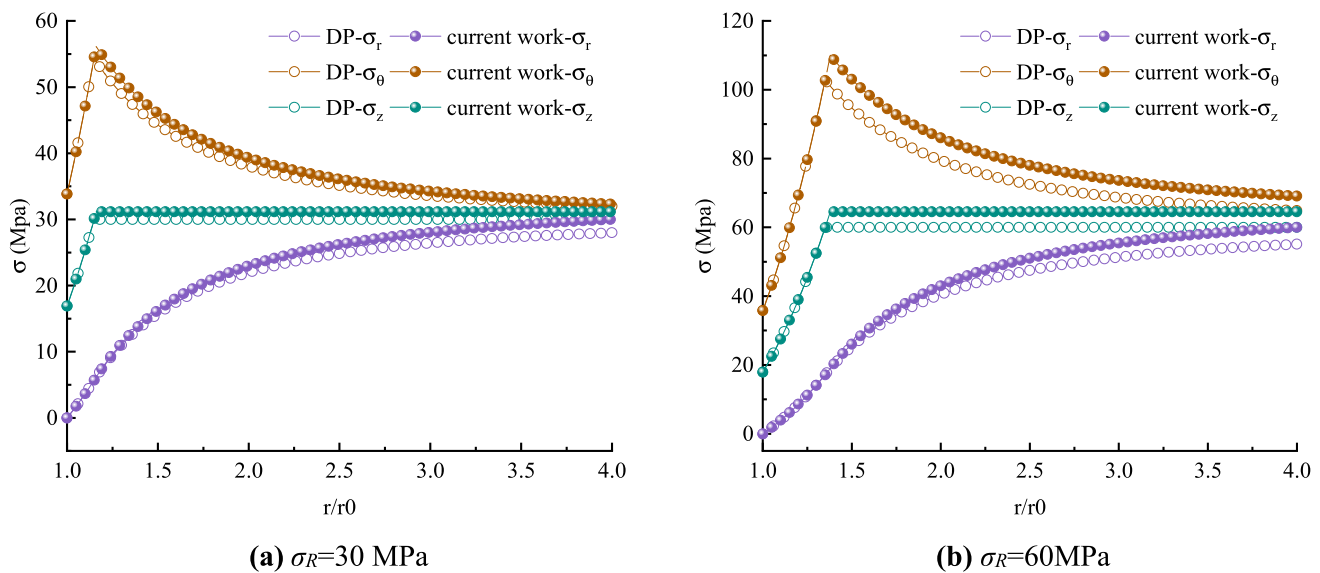


Fig. 5 FLAC3D computational model and results



**Fig. 6** Comparison of stress distribution between FLAC3D and current work



**Fig. 7** Comparison of stress distribution between DP and current work

pressure  $P_0 = 0$ . The parameter  $N = \frac{1+\sin(\phi)}{1-\sin(\phi)}$ ,  $S = \frac{2\sin(\phi)}{1-\sin(\phi)}$  in Kastner's solution.

(2) The relationship between primary rock stress, internal friction angle  $\phi$ , and outer boundary pore water pressure  $P_R$  at yielding condition is shown in Fig. 9. The figure further explains the relationship between the solution in this paper and the solution of DP. The curves are obtained by taking 0, 20, 40, 60, and 80 MPa pore water pressure at

$r_R$ . This seepage force caused by pressure potential energy is the main difference between the work in this paper and the DP solution. In the case of  $P_R = 0$ , the obtained curve is the same to that of DP curve. It can be seen from the analysis results that a higher  $P_R$  value requires a higher yield stress under the same conditions.

In addition, the internal friction angle has a positive effect on the stability of surrounding rock when  $\phi$  is less than  $40^\circ$ , and a negative effect on the stability of

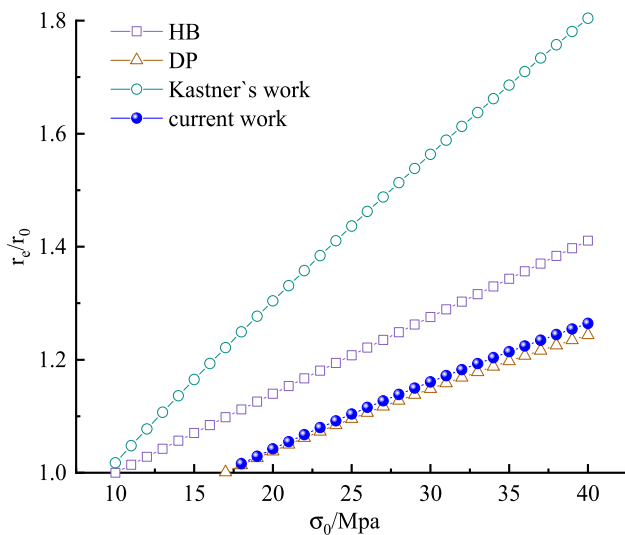


Fig. 8 Influence of confining pressure on radius of plastic zone

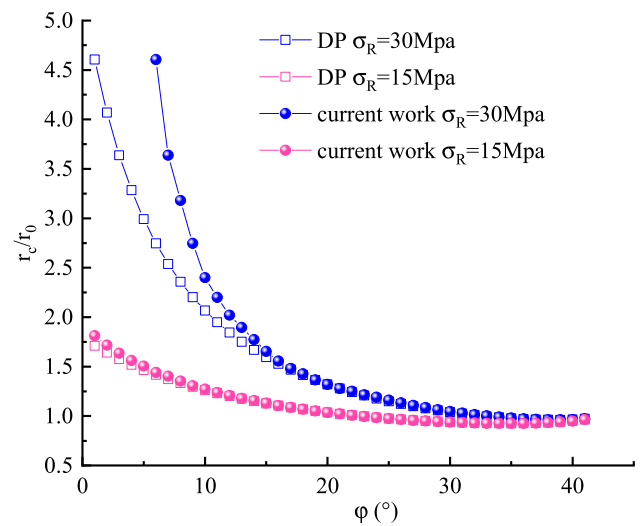


Fig. 10 Relation between internal friction angle and radius of plastic zone

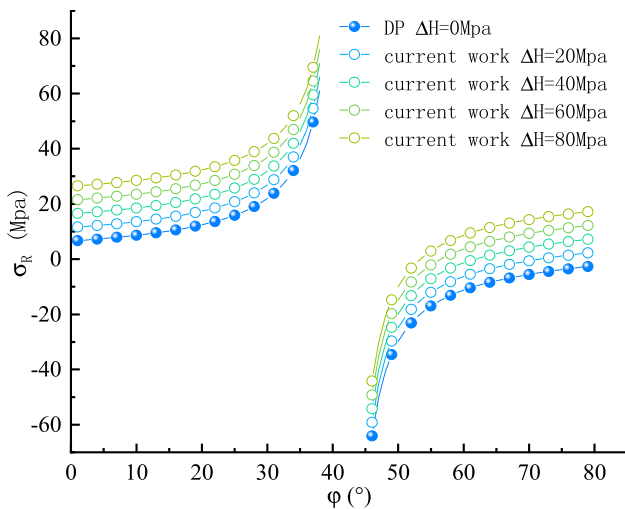


Fig. 9. In-situ stress at initial yield

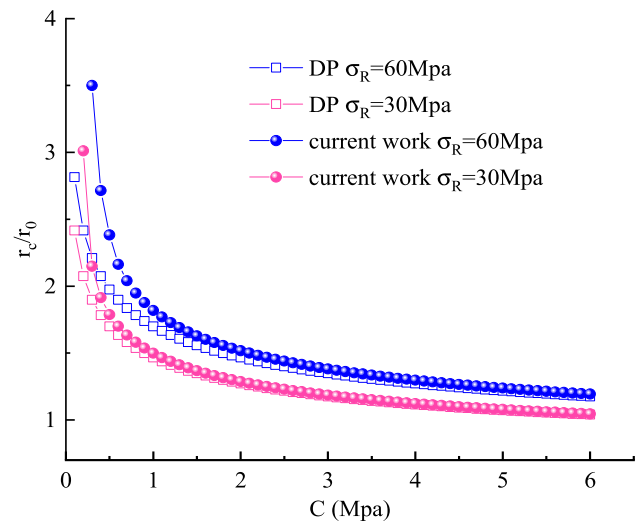


Fig. 11 Relationship between cohesion and radius of plastic zone

surrounding rock when  $\varphi$  is over  $45^\circ$ , showing the characteristics of tensile failure.

In the range of  $40^\circ < \varphi < 45^\circ$ ,  $\sigma_R$  has a high sensitivity to  $\varphi$ . Therefore, the solution proposed in this paper is more reasonable when the internal friction  $\varphi < 40^\circ$ .

(3) The sensitivity analysis between the radius rate of the plastic zone and the internal friction angle of surrounding rock is shown in Fig. 10. According to the proposed criterion, the radius of the plastic zone shows a higher sensitivity at low friction angles, and this sensitivity is more obvious at high stress regions. And the solution presented in this paper shows higher sensitivity. With the increase of in-situ stress, the solution presented in this paper presents a larger range of plastic zone than that presented in the

solution of DP. This phenomenon is most obvious at low angles and tends to be equal with the increase of angles.

(4) Figure 11 shows the relationship between cohesion  $C$  and the radius rate of the plastic zone. Similar to the influence of the internal friction angle  $\varphi$ , the radius of the plastic zone shows a high sensitivity when the cohesion is low (mainly when  $C < 1$  MPa). Similarly, due to the effect of pore water pressure, the solution in this paper shows a higher plastic zone range than that of DP, and this enhancement diminishes with increasing cohesion  $C$ . No matter the DP criterion or the solution in this paper, it can be seen that the influence of in-situ stress on the plastic radius is linear, which is different from the study of internal friction angle  $\varphi$ .

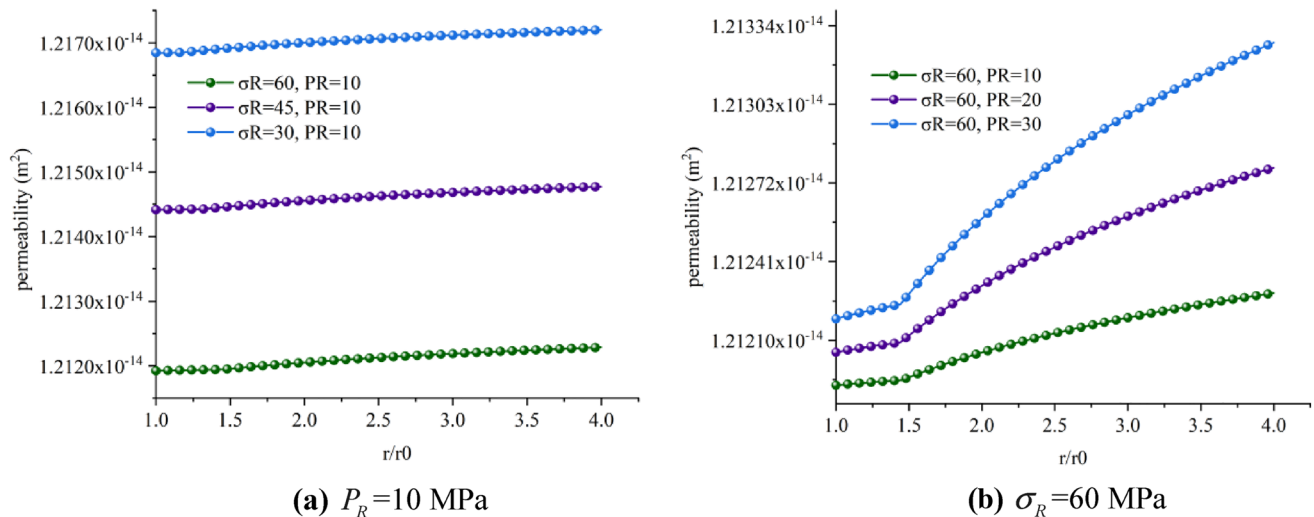


**Fig. 12** Distribution of permeability

(5) Figure 12 shows the distribution of permeability under different in-situ rock stress  $\sigma_R$  and different water pressure  $P_R$ . In this example,  $k_0 = 1 \times 10^{-14} \text{ m}^2$ ,  $n_0 = 0.2$ , inner boundary water head and pressure are set as zero. The outer boundary is applied with water pressure and stress. The distribution of permeability is related to the location of the elastoplastic interface and shows different patterns in different areas. Due to the effect of compressive stress, the closer to the hole, the lower the permeability. The permeability curve has a faster rate of decline in the elastic zone than that in the plastic zone due to the assumption of incompressibility of the plastic volume. In the plastic zone, the volume strain is constant; only the water pressure acts on the volume change of the pores, so that the permeability coefficient decreases slowly. Figure 12a shows a gradual decrease in permeability as  $\sigma_R$  increases, with the permeability curves nearly parallel to each other. Figure 12b shows that the permeability decreases as the  $P_R$  increases and the slope of the permeability curve increases. Comparison of Fig. 12a, b leads to the conclusion that the in-situ rock stress  $\sigma_R$  is the main factor influencing the magnitude of the average permeability and the outer boundary water pressure  $P_R$  is the main factor influencing the distribution of permeability along the penetration path.

## 6 Conclusions

Based on DP criterion and effective stress principle, an elastoplastic fluid–solid model of annular cavity with steady flow is proposed. The model considers the dynamic evolution of the permeability coefficient in the fluid–structure coupling and gives the evolution equations of the permeability coefficient in the elastic and plastic zones and the seepage

equations. In addition, the physical equation of equivalent permeability coefficient and water head difference is considered. By comparing the analytical solution of DP with the numerical simulation of water-rich surrounding rock, the correctness of the proposed solution is verified.

With the increase of primary rock stress, the plastic radius increases significantly, and the solution presented in this paper shows a faster rate of increase than the solution of DP. Due to the consideration of the influence of intermediate principal stress, the solution presented in this paper and the solution of DP require higher ground stress to make the surrounding rock yield. The increase of pore water pressure leads to a higher yield stress of surrounding rock. However, when the pore water pressure decreases gradually and the region is zero, the solution of the elastic region deforms to the classical Lamé solution, while the solution of the plastic region is consistent with the solution of DP.

**Acknowledgements** This research was supported by National Natural Science Foundation of China (Nos. 52264006, 52004072, 52064006, and 52164001), the Guizhou Provincial Science and Technology Foundation (Nos. [2020]4Y044, [2021]292, [2021]N404, and GCC[2022]005-1), Youth Science and technology Talents Development Project of Guizhou Ordinary Colleges and Universities (No. [2022]140), and Specialized Research Funds of Guizhou University (Grant Nos. 201903, 202011).

**Data availability** The data that support the findings of this study are available on request from the corresponding author Chaolin Wang (chaolinwang@126.com), upon reasonable request.

## Declarations

**Conflict of Interest** The authors declared that they have no conflicts of interest to this work. We declare that we do not have any commercial or associative interest that represents a conflict of interest in connection with the work submitted.



## References

- Biot MA (1941) General theory of three-dimensional consolidation. *J Appl Phys* 12:155–164
- Bobet A (2010) Characteristic curves for deep circular tunnels in poro-plastic rock. *Rock Mech Rock Eng* 43:185–200. <https://doi.org/10.1007/s00603-009-0063-z>
- Chen Y, Zhou C, Sheng Y (2007) Formulation of strain-dependent hydraulic conductivity for a fractured rock mass. *Int J Rock Mech Min Sci* 44:981–996. <https://doi.org/10.1016/j.ijrmmms.2006.12.004>
- De Caro M, Crosta GB, Prevati A (2020) Modelling the interference of underground structures with groundwater flow and remedial solutions in Milan. *Eng Geol* 272:105652. <https://doi.org/10.1016/j.enggeo.2020.105652>
- Detournay E, Cheng AHD (1988) Poroelastic response of a borehole in a non-hydrostatic stress field. *Int J Rock Mech Min Sci Geomech Abstr* 25(3):171–182. [https://doi.org/10.1016/0148-9062\(88\)92299-1](https://doi.org/10.1016/0148-9062(88)92299-1)
- Dong X, Karrech A, Qi C, Elchalakani M, Basarir H (2019) Analytical solution for stress distribution around deep lined pressure tunnels under the water table. *Int J Rock Mech Min Sci* 123:104124. <https://doi.org/10.1016/j.ijrmmms.2019.104124>
- Fahimifar A, Zareifard MR (2009) A theoretical solution for analysis of tunnels below groundwater considering the hydraulic–mechanical coupling. *Tunn Undergr Space Technol* 24:634–646
- Fahimifar A, Zareifard MR (2013) A new closed-form solution for analysis of unlined pressure tunnels under seepage forces: analysis of pressure tunnels. *Int J Numer Anal Methods Geomech* 37:1591–1613. <https://doi.org/10.1002/nag.2101>
- Fransson A, Viola G (2021) Bentonite rock interaction experiment: a hydro-structural-mechanical approach. *Eng Geol* 281:105985. <https://doi.org/10.1016/j.enggeo.2020.105985>
- Kabwe E, Karakus M, Chanda EK (2020) Proposed solution for the ground reaction of non-circular tunnels in an elastic-perfectly plastic rock mass. *Comput Geotech* 119:103354. <https://doi.org/10.1016/j.compgeo.2019.103354>
- Kolymbas D, Wagner P (2007) Groundwater ingress to tunnels—the exact analytical solution. *Tunn Undergr Space Technol* 22:23–27
- Lee SW, Jung JW, Nam SW, Lee IM (2007) The influence of seepage forces on ground reaction curve of circular opening. *Tunn Undergr Space Technol* 22:28–38. <https://doi.org/10.1016/j.tust.2006.03.004>
- Li B, Zhang H, Luo Y, Liu L, Li T (2022a) Mine inflow prediction model based on unbiased Grey–Markov theory and its application. *Earth Sci Inf* 15:1–8. <https://doi.org/10.1007/s12145-022-00770-2>
- Li B, Zhang W, Long J, Fan J, Chen M, Li T, Liu P (2022b) Multi-source information fusion technology for risk assessment of water inrush from coal floor karst aquifer. *Geomat Nat Haz Risk* 13:2086–2106. <https://doi.org/10.1080/19475705.2022.2108728>
- Sharan SK (2005) Exact and approximate solutions for displacements around circular openings in elastic–brittle–plastic Hoek–Brown rock. *Int J Rock Mech Min Sci* 42:542–549
- Shin YJ, Kim BM, Shin JH, Lee IM (2010) The ground reaction curve of underwater tunnels considering seepage forces. *Tunn Undergr Space Technol* 25:315–324. <https://doi.org/10.1016/j.tust.2010.01.005>
- Shin JH, Lee IM, Shin YJ (2011) Elasto-plastic seepage-induced stresses due to tunneling. *Int J Numer Anal Meth Geomech* 35(13):1432–1450. <https://doi.org/10.1002/nag.964>
- Wang Y, Dusseault MB (1994) Stresses around a circular opening in an elastoplastic porous medium subjected to repeated hydraulic loading. *Int J Rock Mech Min Sci Geomech Abstr* 31:597–616. [https://doi.org/10.1016/0148-9062\(94\)90003-5](https://doi.org/10.1016/0148-9062(94)90003-5)
- Wang S, Elsworth D, Liu J (2013) Permeability evolution during progressive deformation of intact coal and implications for instability in underground coal seams. *Int J Rock Mech Min Sci* 58:34–45. <https://doi.org/10.1016/j.ijrmmms.2012.09.005>
- Wang CL, Zhang KP (2022a) An adsorption model for cylindrical pore and its method to calculate pore size distribution of coal by combining NMR. *Chemical Engineering Journal* 450:138415. <https://doi.org/10.1016/j.cej.2022.138415>
- Wang CL, Zhao Y, Ning L, Bi J (2022b) Permeability evolution of coal subjected to triaxial compression based on in-situ nuclear magnetic resonance. *Int J Rock Mech Min Sci* 159:105213
- Xu Z, Xu X, Lu B (2000) An analytical solution for elastoplastically nonlinear seepage coupling. *J Chongqing Univ (Nat Sci Ed)* s1:184–187 (in Chinese)
- Xu P, Yang SQ (2016) Permeability evolution of sandstone under short-term and long-term triaxial compression. *Int J Rock Mech Min Sci* 85:152–164. <https://doi.org/10.1016/j.ijrmmms.2016.03.016>
- Yang SQ, Huang YH, Jiao YY, Zeng W, Yu QL (2015) An experimental study on seepage behavior of sandstone material with different gas pressures. *Acta Mech Sin* 31:837–844. <https://doi.org/10.1007/s10409-015-0432-7>
- Zareifard MR, Fahimifar A (2014) Effect of seepage forces on circular openings excavated in Hoek–Brown rock mass based on a generalised effective stress principle. *Eur J Environ Civ Eng* 18:584–600
- Zhang B, Chen F, Wang Q (2019) Elastoplastic solutions for surrounding rock masses of deep-buried circular tunnels with non-darcian flow. *Int J Geomech* 19:04019065
- Zhao CX, Zhang ZX, Lei QH (2021) Role of hydro-mechanical coupling in excavation-induced damage propagation, fracture deformation and microseismicity evolution in naturally fractured rocks. *Eng Geol* 289:106169
- Zhao Y, Zhang YF, Tian G, Wang CL, Bi J (2022) A new model for predicting hydraulic fracture penetration or termination at an orthogonal interface between dissimilar formations. *Petroleum Science* 19(6): 2810–2829. <https://doi.org/10.1016/j.petsci.2022.08.002>
- Zhang YF, Long AF (2023) Mutual impact of true triaxial stress borehole orientation and bedding inclination on laboratory hydraulic fracturing of Lushan shale. *Journal of Rock Mechanics and Geotechnical Engineering* <https://doi.org/10.1016/j.jrmge.2023.02.015>

**Publisher's Note** Springer Nature remains neutral with regard to jurisdictional claims in published maps and institutional affiliations.

Springer Nature or its licensor (e.g. a society or other partner) holds exclusive rights to this article under a publishing agreement with the author(s) or other rightsholder(s); author self-archiving of the accepted manuscript version of this article is solely governed by the terms of such publishing agreement and applicable law.